Multi-scenario interpretations from sparse fault evidence using graph theory and geological rules

Gabriel Godefroy, Guillaume Caumon, Gautier Laurent, François Bonneau

Multi-scenario interpretations from sparse fault evidence using graph theory and geological rules

Gabriel Godefroy [1], Guillaume Caumon [1], Gautier Laurent [1,2], and François Bonneau [1]

[1] Université de Lorraine, CNRS, GeoRessources, ENSG
[2] Univ. Orléans, CNRS, BRGM, ISTO, UMR 7327
[1]F-54000 Nancy, France
[2]F-45071, Orléans, France

Key Points:

- Several plausible scenarios can be made when interpreting faulted structures from sparse subsurface data.
- From numerical rules expressing conceptual knowledge, a graph-based sampler generates several possible fault scenarios honoring spatial data.
- Numerical experiments suggest that the use of coherent interpretation rules increases the likelihood of generating correct interpretations.

Corresponding author: Gabriel Godefroy, `Gabriel.Godefroy@hotmail.fr`

Abstract

The characterization of geological faults from geological and geophysical data is often subject to uncertainties, owing to data ambiguity and incomplete spatial coverage. We propose a stochastic sampling algorithm which generates fault network scenarios compatible with sparse fault evidence while honoring some geological concepts. This process proves useful for reducing interpretation bias, formalizing interpretation concepts, and assessing first-order structural uncertainties. Each scenario is represented by an undirected association graph, where a fault corresponds to an isolated clique, which associates pieces of fault evidence represented as graph nodes. The simulation algorithm samples this association graph from a possibility graph, whose edges represent the independent association of any two pieces of fault evidence. Each edge carries a likelihood that the endpoints belong to the same fault surface is computed, expressing general and regional geological interpretation concepts. The algorithm is illustrated on several incomplete data sets made of three to six two-dimensional seismic lines extracted from a three-dimensional seismic image located in the Santos Basin, offshore Brazil. In all cases, the simulation method generates a large number of plausible fault networks, even when using restrictive interpretation rules. The case study experimentally confirms that retrieving the reference association is tedious due to the problem combinatorics. Restrictive and consistent rules increase the likelihood to recover the reference interpretation and reduce the diversity of the obtained realizations. We discuss how the proposed method fits in the quest to rigorously (1) address epistemic uncertainty during structural uncertainty studies and (2) quantify subsurface uncertainty while preserving structural consistency.

Plain Language Summary

This paper presents a way to generate interpretation scenarios for geological faults from incomplete spatial observations. The method essentially solves a "connect the dots" exercise that honors the observations and geological interpretation concepts formulated as mathematical rules. The goal is to help interpreters to characterize how the lack of data affects geological structural uncertainty. The proposed method is original in the sense that it does not anchor the scenarios on a particular base case, but rather uses a global characterization formulated with graph theory to generate possible fault network interpretations. The application on a faulted formation offshore Brazil where observations have been decimated, shows that the method is able to consistently generate a set of interpretations encompassing the interpretation made from the full data set. It also highlights the computational challenge of the problem and the difficulty to check the results in settings where only incomplete observations exist. The proposed method, however, opens novel perspectives to address these challenges.

1 Introduction

Introduction

In structural characterization of geophysical data and geological mapping, the lack of conclusive observations generally makes interpretation necessary to obtain a consistent subsurface model. Indeed, geological observations and geophysical signals often have an incomplete spatial coverage and non-unique interpretations due to a lack of resolution or physical ambiguities (Wellmann & Caumon, 2018). As a result, structural uncertainty often remains after interpretation, and it affects fundamental research on earth's structure such as, for example, the understanding of rift development and earthquake processes (Mai et al., 2017; Riesner et al., 2017; Sepúlveda et al., 2017; Zakian et al., 2017; Gombert et al., 2018; Ragon et al., 2018; Tal et al., 2018). Structural uncertainty also impacts applied studies, for example on natural resource exploration and exploitation (Hollund et al., 2002; Julio et al., 2015a; Richards et al., 2015; Rivenæs et al., 2005; Seiler et al., 2010; Thore et al., 2002), waste disposal (Mann, 1993; Schneeberger et al., 2017),

environmental engineering (Rosenbaum & Culshaw, 2003), civil engineering works (Zhu et al., 2003). In all these applications, faults are often the source of significant geometrical and petrophysical complexity, as fault zones often have distinct hydromechanical properties, and also because fault displacement controls the geometric layout of rock units in the subsurface. Understanding and reducing fault uncertainty is, therefore, essential in many geoscience studies.

To characterize structural uncertainty, one may ask a population of geologists to interpret a particular data set (e.g., Bond et al., 2007; Schaaf & Bond, 2019). However, interpreting a subsurface data set in three dimensions commonly takes up to several months, so this strategy is difficult to generalize. Alternatively, one may use computing power assess uncertainty in structural models. For this, stochastic structural modeling has already been proposed to generate several scenarios while taking account of seismic image quality and faults below seismic resolution (Aydin & Caers, 2017; Hollund et al., 2002; Holden et al., 2003; Irving et al., 2010; Julio et al., 2015a, 2015b; Lecour et al., 2001); uncertainty related to reflection seismic acquisition and processing (Osypov et al., 2013; Thore et al., 2002); geological field measurement uncertainty (Jessell et al., 2014; Lindsay et al., 2012; Pakyuz-Charrier et al., 2019; Wellmann et al., 2014); structural parameters for folding (Grose et al., 2019, 2018); and observation gaps (Aydin & Caers, 2017; Cherpeau et al., 2010b; Cherpeau & Caumon, 2015; Holden et al., 2003). Considering several structural interpretations has also proved useful to propagate uncertainties to flow simulations (Julio et al., 2015b), to rank structural models against physical data and ultimately to falsify some of the interpretations using a Bayesian approach (Cherpeau et al., 2012; de la Varga & Wellmann, 2016; Irakarama et al., 2019; Seiler et al., 2010; Suzuki et al., 2008; Tarantola, 2006; Wellmann et al., 2014). In the above approaches, several conceptual models are used to describe structural uncertainties. A general research question is whether the methods produce "geologically realistic" models, what this term actually means, and how it can be effectively embedded in conceptual models of uncertainty (Caumon, 2010; de la Varga & Wellmann, 2016; Jessell et al., 2010, 2014; Thibaut et al., 1996; Wellmann & Caumon, 2018).

During the interpretation of faults from sparse observations, the choice of a particular conceptual model can be consequential to explore and reduce uncertainties. Faults are typically inferred from observations made on outcrops, wells, geophysical images, or through the inversion of focal mechanisms. Classically, the interpretation of these data is translated into points, lines or surfaces indicating the fault position and orientation. These geometric interpretations (*fault evidence* or *fault data*) may themselves be uncertain (existence, geometry, connectivity). The problem of modeling geologically realistic fault structures from such incomplete fault data has been initially described by Freeman et al. (1990) (Figure 1a,b,c), who proposed a methodology based on displacement analysis to help geologists manually choose between various fault scenarios.

Generating these scenarios, however, needs efficient computational techniques to explore the possibility space. Statistical point processes provide a general mathematical framework for this (Holden et al., 2003). As tectonic history places specific constraints on fault networks in terms of orientation and truncation patterns, it is possible to represent each fault surface as a level set and to sequentially simulate fault sets to reproduce specific statistics for each fault set, while enforcing abutting relationships between the simulated faults (Aydin & Caers, 2017; Cherpeau et al., 2010b, 2012; Cherpeau & Caumon, 2015). For honoring spatial fault data, Aydin and Caers (2017) use an extended Metropolis sampler which, at each stage of the simulation, adds, removes, or modifies a fault object. This sampler has theoretical convergence properties, but simulating fault networks in the presence of a large number of fault data remains computationally challenging. Therefore, Cherpeau et al. (2010b, 2012) and Cherpeau and Caumon (2015) propose a parsimonious method which anchors the first simulated faults to the available evidence, before simulating unseen fault objects. All these iterative stochastic fault mod-

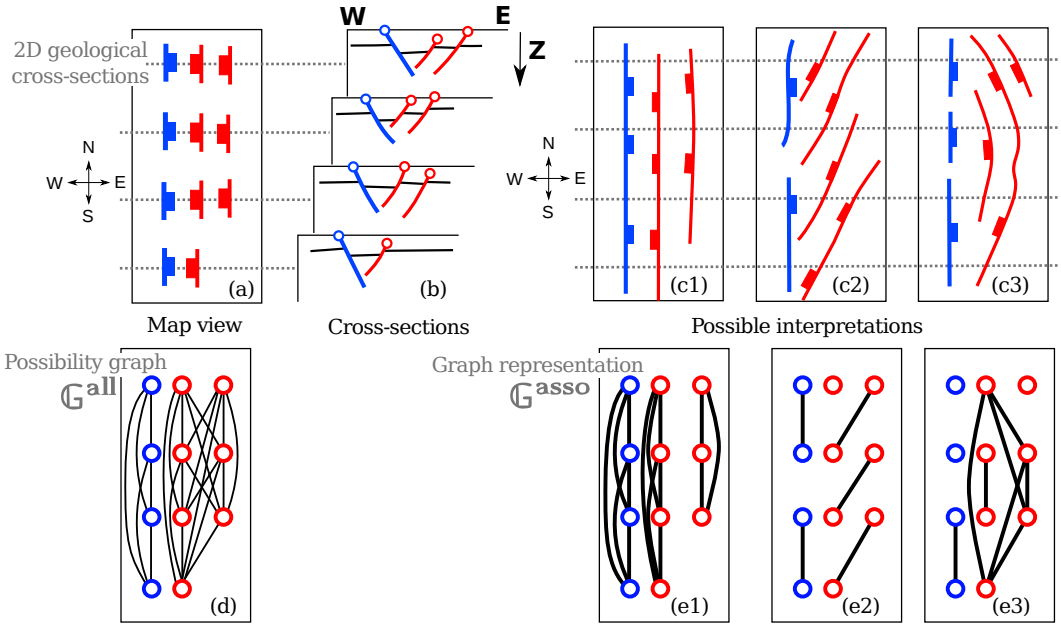

Figure 1. Associating labeled pieces of fault evidence (red: east-dipping and blue: west-dipping) interpreted (a) in map view or (b) on two-dimensional seismic lines is an under-constrained problem. (c_1, c_2 and c_3) Several structural interpretations are possible (Modified from Freeman et al., 1990; Godefroy et al., 2019). (d) In a possibility graph ($\mathbb{G}^{\mathbf{all}}$), the labeled nodes (i.e., the pieces of fault evidence) are linked by an edge if they may be part of the same fault. (e_1, e_2 and e_3) Plausible interpretations are represented by an association graph where the edges link pieces of fault evidence interpreted as belonging to the same fault.

els are difficult to use in practice, primarily because of the combinatorial complexity of the problem (Godefroy et al., 2019; Julio, 2015), of the difficulty to integrate geological, kinematical and mechanical concepts into the stochastic model (Godefroy et al., 2017; Laurent et al., 2013; Nicol et al., 2020; Røe et al., 2014; Rotevatn et al., 2018), and of the geometric challenges to robustly build such three-dimensional structural models (e.g., due to meshing issues, see Anquez et al., 2019; Zehner et al., 2015).

This paper focuses on the combinatorial problem, as it is a prerequisite to address the other challenges. For this, we split stochastic structural simulation into three sub-problems: (1) The *fault data association problem* (also termed fault correlation by Freeman et al., 1990), which aims at determining which of the pieces of evidence may belong to the same fault; (2) The interpolation problem, which determines fault geometry and displacement from available data, and which has been extensively addressed in deterministic geological modeling (see Section 3 of Wellmann & Caumon, 2018, and references therein); (3) The simulation of unobserved structures, which can be addressed by appropriate statistical point processes (Aydin & Caers, 2017; Cherpeau et al., 2010b; Holden

et al., 2003). As items (2) and (3) have already received attention, this contribution focuses on finding a suitable computational method for solving the data association problem. For this, we build on a recent formalism (Godefroy et al., 2019), where an association scenario is represented by an undirected graph ($\mathbb{G}^{\mathbf{asso}}$, Figure 1.e). In this graph, each labeled node represents one piece of fault evidence and each edge associates two nodes belonging to the same fault. Each connected component represents a fault, and is necessarily a complete subgraph (or clique) of $\mathbb{G}^{\mathbf{asso}}$: all the nodes of a connected component are mutually connected. $\mathbb{G}^{\mathbf{asso}}$ is a subset of a much larger possibility graph $\mathbb{G}^{\mathbf{all}}$, which describes all possible pairwise associations of the available pieces of evidence (Figure 1.d). A key idea of Godefroy et al. (2019) is to assign weights to the edges of $\mathbb{G}^{\mathbf{all}}$, to represent the likelihood that any pair of fault data belongs to the same fault object based on prior geological knowledge. Below a certain likelihood, the edge can be removed, which significantly reduces the number of possible scenarios. The analysis of maximal cliques in this simplified graph provides fault association scenarios, but the ability of the approach to sensibly sample fault uncertainty has not been demonstrated.

In the present contribution, we propose a stochastic graph decomposition algorithm to automate the generation of several possible fault scenarios (or, equivalently, graphs $\mathbb{G}^{\mathbf{asso}}$) from an input graph $\mathbb{G}^{\mathbf{all}}$ representing fault data and structural knowledge (Section 2). A lightweight graph data structure carries the structural interpretation and enables to generate millions of alternative models. To study the properties of the model space sampled by this algorithm, we consider a reference model built from high-resolution seismic data, offshore Brazil, and extract from this reference model several sparse data sets of variable density. We combine several likelihood criteria translating varying degrees of geological knowledge to check the consistency of the method (Section 3). We then discuss how this approach may help address some longstanding challenges for integrating data and knowledge and better understand brittle structures in the Earth's crust (Section 4).

2 Multi-scenario interpretations using graph decomposition

In the graph framework proposed by Godefroy et al. (2019), the simulation of fault network scenarios amounts to decomposing the possibility graph $\mathbb{G}^{\mathbf{all}}$ into a graph $\mathbb{G}^{\mathbf{asso}}$ composed solely of disjoint cliques (i.e., fully connected sets of nodes) corresponding to fault surfaces. This means that simulating likely fault networks using this formalism is equivalent to generating random decompositions of the graph $\mathbb{G}^{\mathbf{all}}$ into a set of cliques. Several graph clustering methods are available in the literature (e.g., Schaeffer, 2007). These algorithms generally provide one single decomposition and are thus not directly applicable to uncertainty assessment by stochastic simulation. Before explaining the proposed decomposition algorithm, we first describe how information can be attached to the graph nodes and edges to represent geological concepts.

2.1 Accounting for geological knowledge

As the number of fault data for a given area can be very large, we propose to use the concept of fault families to reduce the number of possible associations, as done classically in fracture and fault analysis (e.g., Cherpeau et al., 2010b; Henza et al., 2011; Nixon et al., 2011). Indeed, regional geological knowledge generally includes a description of tectonic phases through time, which can be translated in terms of statistical descriptions for fault and fracture families. Each piece of fault evidence may be, in this context, labeled by a probability to belong to a particular fault family. Family rules $R_{\varphi}^{\mathbf{fam}}(\mathbb{v}_i)$ quantify the likelihood that a fault data $\mathbb{v}_i$ belongs to the given family denoted by the index φ (Godefroy et al., 2019). Family rules attach to each piece of evidence a number be-

tween 0 (if $\mathbb{v}_i$ cannot belong to the fault family φ) and 1 (if it is highly likely that $\mathbb{v}_i$ belongs to the fault family φ). This score is attributed by comparing semantic information about a piece of fault evidence, stored in the form of node labels, and general prior information about a given fault family. The node labels may carry kinematic characteristics, such as the observed fault type (for example normal or reverse) or the apparent orientation of interpreted fault lines.

As a simple example, the colors in Figure 1 reflect a deterministic assignment of all graph nodes to west-dipping or east-dipping fault families. In the graph formalism, this means that the global association graph can be decomposed into several disjoint association subgraphs:

$$\mathbb{G}^{\mathbf{asso}} = \bigcup_{\varphi=1}^{\varphi=n} \mathbb{G}_{\varphi}^{\mathbf{asso}}, \tag{1}$$

where n is the number of fault families ($n = 2$ in Figure 1.e). Each association scenario corresponds in turn to a decomposition of each subgraph $\mathbb{G}_{\varphi}^{\mathbf{asso}}$ into a set of isolated cliques. In the possibility graph $\mathbb{G}^{\mathbf{all}}$, the decomposition into family subgraphs $\mathbb{G}_{\varphi}^{\mathbf{all}}$ may also be based on family tags attached to each piece of fault evidence (Figure 1.d). Note that in this case, the subgraphs $\mathbb{G}_{\varphi}^{\mathbf{all}}$ may not always be disjoint. Indeed, a node corresponding to a piece of fault evidence may belong to several fault families, hence to several possibility subgraphs.

To further include geological knowledge in the simulator, an association rule $R_{\varphi}^{\mathbf{assoc}}(\mathbb{v}_i \leftrightarrow \mathbb{v}_j)$ quantifies the likelihood that two pieces of evidence ($\mathbb{v}_i$ and $\mathbb{v}_j$) of the same family (φ) belong to the same fault (Godefroy et al., 2019). An association rule $R_{\varphi}^{\mathbf{assoc}}(\mathbb{v}_i \leftrightarrow \mathbb{v}_j)$ returns a number between 0 ($\mathbb{v}_i$ and $\mathbb{v}_j$ cannot belong to the same fault of the family φ) and 1 (if both fault data are likely to belong to the same fault). Association rules are defined from general structural concepts about faults and from some geometric characteristics associated with each fault family. For example, it can rely on the distance between the evidence, the consistency between the fault family orientation and the orientation of the edge connecting two pieces of evidence (Cherpeau & Caumon, 2015), the throw gradient along the fault (e.g., Barnett et al., 1987; Freeman et al., 1990; Cherpeau & Caumon, 2015), or the estimated separation across a faulted area (Freeman et al., 2010).

2.2 Size of the search space

From a combinatorial standpoint, the total number of association scenarios of n fault data is equal to the Bell number B_n, which correspond to the number of partitions of a complete graph (Godefroy et al., 2019). When rules and families remove edges in $\mathbb{G}^{\mathbf{all}}$, the graph becomes incomplete and the Bell number significantly overestimates the number of possible association scenarios. For example, without making any assumption or geometric consideration, the total number of possible scenarios for associating the 11 fault data in Figure 1 would be equal to $B_{11} = 678,570$. The definition of two disjoint families containing 4 and 7 pieces of evidence reduces this number to $B_4 \times B_7 = 13,155$.

In the general case, however, the graph $\mathbb{G}^{\mathbf{all}}$ is incomplete; it is currently impossible to perform a more accurate combinatorial analysis just by considering the structure of the graph $\mathbb{G}^{\mathbf{all}}$. Upper bounds have been proposed for the number of cliques in an arbitrary graph (e.g., theorem 3 in Wood, 2007), but not for the number of graph partitions into *disjoint* cliques. This difficulty impacts the evaluation of results produced by any uncertainty quantification method, as the size of the search space cannot be evaluated without solving the highly challenging problem of explicitly listing all the possible configurations (Knuth, 2005).

2.3 Sampling by stochastic graph partitioning

To generate several scenarios, we propose a hierarchical method relying on sets of nodes that are all connected (cliques) in the possibility graph of at least one family $\mathbb{G}_{\varphi}^{\mathbf{all}}$. In graph theory, cliques that cannot be enlarged without adding new edges are maximal cliques. Maximal cliques can be detected using the Bron-Kerbosch algorithm (Bron & Kerbosch, 1973). Maximal cliques are used at the beginning of the process in order to mimic a manual interpretation where the geologist starts by interpreting the major structures.

Choice of parameters: based on the available data, pieces of fault evidence are digitized and represented as graph nodes. The method has been developed within the SKUA-GOCAD environment (Emerson, 2018) and takes advantage of the available data structures, so every graph node can be attached to a set of points, lines, or triangulated surfaces describing fault evidence geometry. Information attached to these pieces of evidence, such as apparent throw or orientation, are stored as node labels. For each fault family, a family rule and an association rule expressing prior geological knowledge are defined (Figure 2, step 1).

Creation and segmentation of the possibility graph: the family and association rules are used to compute a graph of all possible associations $\mathbb{G}_{\varphi}^{\mathbf{all}}$ for each family φ (Godefroy et al., 2019) (Figure 2, step 2.1). A wide range of formulas can be used to compute the likelihoods according to the defined rules. Each edge $\mathbb{e}^{\varphi}(\mathbb{v}_i, \mathbb{v}_j)$ of $\mathbb{G}_{\varphi}^{\mathbf{all}}$ (linking two pieces of evidence $\mathbb{v}_i$ and $\mathbb{v}_j$) carries an association likelihood $L_{\varphi}^{\mathbf{all}}(\mathbb{v}_i \leftrightarrow \mathbb{v}_j)$ for each family φ:

$$L_{\varphi}^{\mathbf{all}}(\mathbb{v}_i \leftrightarrow \mathbb{v}_j) = R_{\varphi}^{\mathbf{fam}}(\mathbb{v}_i)\, R_{\varphi}^{\mathbf{fam}}(\mathbb{v}_j)\, R_{\varphi}^{\mathbf{assoc}}(\mathbb{v}_i \leftrightarrow \mathbb{v}_j). \tag{2}$$

For simplicity, this choice assumes that the events '$\mathbb{v}_i$ belongs to family φ', '$\mathbb{v}_j$ belongs to family φ' and '$\mathbb{v}_i$ and $\mathbb{v}_j$ belongs the same fault' are independent. It ensures that $L_{\varphi}^{\mathbf{all}}(\mathbb{v}_i \leftrightarrow \mathbb{v}_j) = 0$ if either $R_{\varphi}^{\mathbf{fam}}(\mathbb{v}_i) = 0$, $R_{\varphi}^{\mathbf{fam}}(\mathbb{v}_j) = 0$ (e.g., the dip of either pieces of fault evidence does not correspond to the dip of the family φ), or $R_{\varphi}^{\mathbf{assoc}}(\mathbb{v}_i \leftrightarrow \mathbb{v}_j) = 0$ (e.g., the locations of $\mathbb{v}_i$ and $\mathbb{v}_j$ are incompatible with the orientation of faults belonging to the family ϕ). The edges where $L_{\varphi}^{\mathbf{all}}(\mathbb{v}_i \leftrightarrow \mathbb{v}_j)$ is null are, therefore, removed from $\mathbb{G}_{\varphi}^{\mathbf{all}}$. This deletion has a strong impact of the simulation results, as the corresponding associations are not considered later, but it significantly reduces the number of acceptable association scenarios (Section 2.2). The major possible structures are then listed using the Bron-Kerbosch algorithm (Bron & Kerbosch, 1973) which finds the maximal cliques in $\mathbb{G}_{\varphi}^{\mathbf{all}}$ (Figure 2, step 2.2).

Stochastic fault association and segmentation: cliques are randomly and sequentially drawn and removed from the current possibility graph until each fault evidence has been assigned to a fault. Several strategies can be defined and chosen for this sequential random selection of faults. To mimic the interpretation process by experts, who tend to first focus on the major structures (e.g., Lines & Newrick, 2004), we propose to preferentially select large and overall likely faults before selecting small and unlikely faults. At each step, the sampling probability of a clique $\mathbb{F} = \{\mathbb{v}_i, ..., \mathbb{v}_j\}$ depends on the number of nodes $|\mathbb{F}|$ and on the mean association likelihood $\overline{L_{\varphi}^{\mathbf{all}}(\mathbb{F})}$ as

$$P_{draw\ struct}(\mathbb{F}) = \frac{\overline{L_{\varphi}^{\mathbf{all}}(\mathbb{F})}\ |\mathbb{F}|^{\alpha_{draw}}}{\sum_{\mathbb{F}}^{\mathtt{all\ cliques}} \overline{L_{\varphi}^{\mathbf{all}}(\mathbb{F})}\ |\mathbb{F}|^{\alpha_{draw}}}, \tag{3}$$

where α_{draw} is used to weight the number of fault evidences in the clique (the structure containing more nodes are more likely to be drawn when α_{draw} increases, see sensitivity study in Section 3.2). Other selection strategies using, for example, the distance separating the pieces of evidence or their sizes could also be used to create large structures.

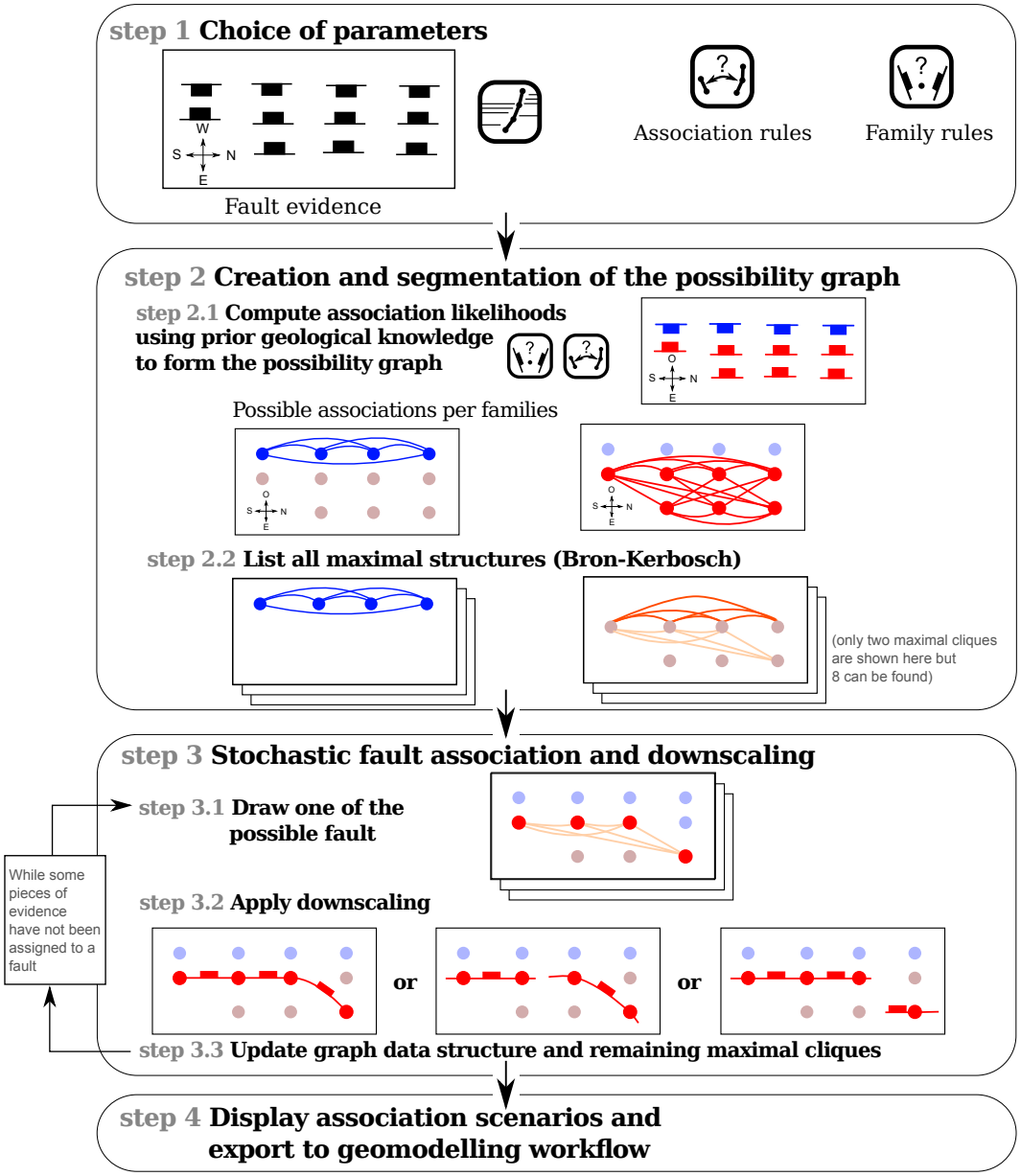

Figure 2. Sequential stochastic algorithm interpreting the available fault data as distinct cliques in $\mathcal{G}_{\varphi}^{\mathbf{all}}$. (step 1) The algorithm requires input fault interpretations and a set of interpretation rules. (step 2.1) Family and association rules are used to compute the graphs $\mathcal{G}_{\varphi}^{\mathbf{all}}$ of all possible associations for each family φ. (step 2.2) The potential major structures (maximal cliques) are detected. (step 3) Iteratively sample some fault objects associating a set of data and update the graph $\mathcal{G}_{\varphi}^{\mathbf{all}}$ and its maximal cliques. (step 4) When all the pieces of evidence have been assigned to fault surfaces, the association scenario can be displayed or used to interpolate or simulate the fault surface geometry.

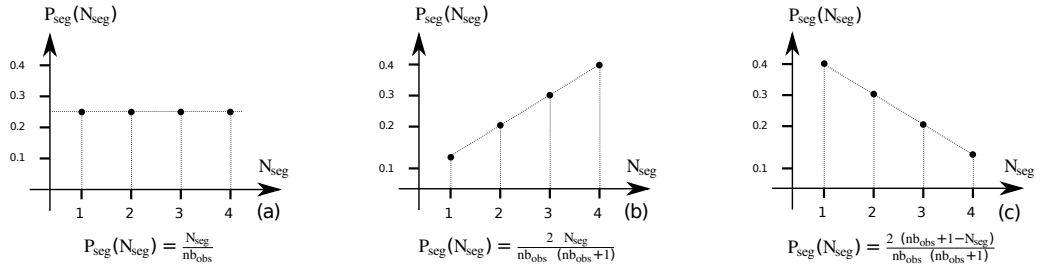

Figure 3. Three probability density functions that can be used to draw the number of segments during the segmentation step: (a) uniform, (b) increasing, and (c) decreasing.

The maximal clique listing is a way to start the interpretation in a parsimonious manner by looking at the major potential structures. However, these potential major structures can be made of several faults or several segments possibly linked by relay zones (e.g., Ferrill et al., 1999; Julio et al., 2015a; Manighetti et al., 2015; Peacock & Sanderson, 1991). These potential fault segments should be considered to completely explore the uncertainty space. For this, we propose a simple procedure to split a fault $\mathbb{F}$ made of $|\mathbb{F}|$ pieces of fault evidence into N_{seg} fault segments; this strategy is called *downscaling* in Julio et al. (2015a, 2015b). For simplicity, the number N_{seg} is drawn randomly in this paper between 1 (no segmentation) and $|\mathbb{F}|$ (each piece of evidence explains one individual fault segment). This random selection relies on a probability law called P_{seg}, which can be either uniform, linearly decreasing or increasing (Figure 3.a, b, c, respectively). A sensitivity analysis is presented in Section 3.2 to show how the choice of P_{seg} impacts the total number of detected structures.

In the above simulation method, faults are simulated independently, and the possibility of interactions is not considered. Indeed, we consider that branch lines are not present in the data, as it is very unlikely that branch lines are directly observed on typical subsurface data (Yielding, 2016). For this reason, we consider that each piece of fault evidence can belong only to one fault surface, so the nodes corresponding to a selected clique are not considered in further simulation steps (Figure 2, step 3.3).

As a result of this process, it is possible that crossing faults are generated by the simulation; in some geological contexts, it might be reasonable to make the hypothesis that fault intersections at large scale are unlikely (as in Schneeberger et al., 2017). When fault data have been interpreted along parallel two-dimensional seismic lines, a labelling is used to detect possible intersections between the simulated fault segments and the remaining cliques. After each downscaling step (step 3.2), the edges crossing the simulated fault are also removed from the remaining cliques while updating the data structure (step 3.3). A similar graph problem is solved using the Dynamic Time Warping algorithm (Levenshtein, 1966) in order to correlate stratigraphic data along wells (Edwards et al., 2018; Lallier et al., 2013; Smith & Waterman, 1980). Note that the proposed strategy to avoid intersections is applicable only in the presence of fault interpretations made on parallel sections. Extending this constraint to irregularly sampled sparse data would require sweeping the possibility graph to traverse the fault data.

Fault surface modeling: the presented strategy generates data association scenarios that are exported into a visual representation (Figure 2, step 4). Each scenario is represented by an association graph where each fault corresponds to a connected

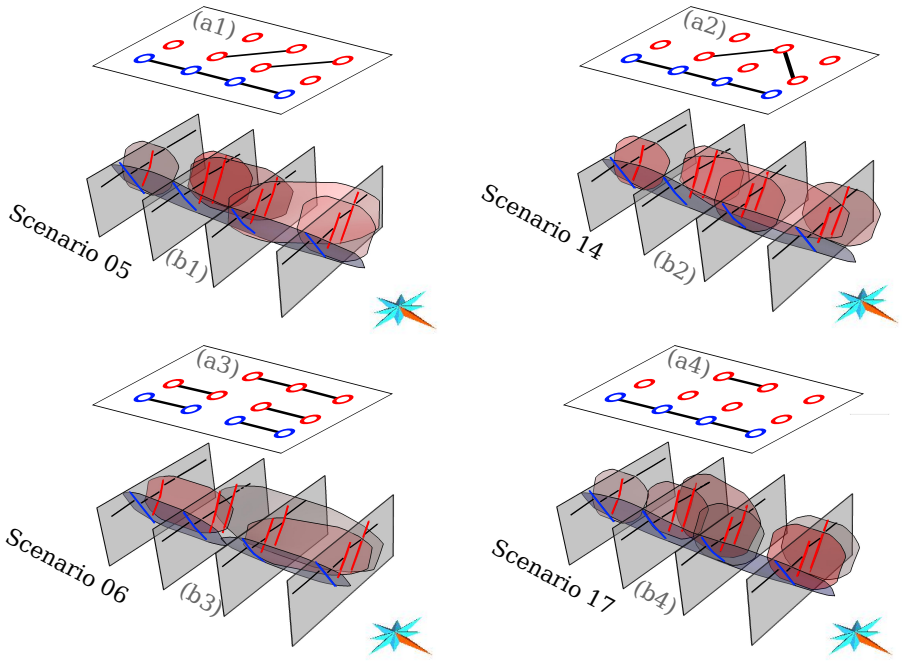

Figure 4. (a) The generated interpretation scenarios are represented by association graphs. (b) For each clique, a fault surface can be interpolated using the geometry of the fault evidence. Data and generated models can be visualized here: `gabrielgodefroy.github.io/StochasticInterpData/Fig4/Fig4.html`

component of the association graph (Figure 4.a). Fault surfaces can then be interpolated from the available evidence (e.g., Mallet, 1992). Our implementation uses the Structure and Stratigraphy workflow of SKUA-GOCAD (Emerson, 2018). This process interpolates each fault surface as the equipotential of a scalar field (Frank et al., 2007). The tip line of each fault is classically obtained taking the convex hull of the fault data, which may then be manually edited by the interpreter (Emerson, 2018). To obtain larger fault extents automatically, we simply compute the ellipsoid containing the data (Figures 4.b and supplementary data). As a refinement, fault extents could be sampled from a probability distribution obtained by updating the prior distribution for the considered fault family with the available information for the current fault data (geometry and observed displacement). The geometric uncertainty around the generated association scenario may be further assessed by data perturbation or surface perturbation (see survey in Section 4 of Wellmann & Caumon, 2018).

3 Application to sparse data from Santos basin, offshore Brazil

We applied the proposed stochastic fault network simulation method on a natural example of faulted structures imaged by three-dimensional seismic data located in the Santos basin, offshore Brasil. The Santos Basin formed during Early Cretaceous when

Table 1. Spacing between the 2D lines used to generate the synthetic data.

Number of lines	3	4	5	6
Spacing	2.9 km	1.90 km	1.45 km	1.16 km

the South Atlantic began to open. The faults grew from Albian to Miocene and from Oligocene to present within Albian Carbonates (Ithanhaem Formation) and within Cenomanian to recent fine-grained clastics (Itajai-Acu and Marambia formations). Fault growth was activated by the mobilization of an underlying salt-rich unit (Ariri Formation). The underlying salt anticlines and salt plateaux can be up to 2.6 km thick (see Tvedt et al. (2016) and references therein for more details).

From the available time-migrated seismic data (see sample section on Figure 5.a), we selected a densely faulted area where we interpreted 27 fault surfaces (see Figure 5.b and Godefroy et al. (2017)). Given the excellent quality of the seismic image, there is very limited structural uncertainty in this interpretation, which is further used as the reference interpretation. From this reference model, we extracted incomplete fault data along several parallel two-dimensional sections to emulate the case of the same area being imaged by two-dimensional seismic lines (Figure 5.c,d).

In the remainder of Section 3, we propose numerical experiments to evaluate the consistency of the model space sampled by the proposed simulation method from these incomplete data sets. Intuitively, a consistent sampling method should, when appropriately parameterized, retrieve the reference association with the maximum frequency. Also, the likelihood to retrieve the reference association should increase as more data and correct informative rules are used. However, in practice, the rules may be biased because of preferential sampling or wrong analog knowledge, so we will also check for the impact of using biased rules on the ability of the method to find the correct association. Finally, in a consistent sampling, the spread of the samples around the reference should also reduce when more information becomes available. However, checking for all these properties is difficult in our case, as the dimension of the problem changes when the number of observations changes. Therefore, we first study how the structure of the association problem changes with the number of fault data and the degree of information brought by geological rules.

3.1 Synthetic two-dimensional lines and geological rules

To quantify the role of a particular geological concept in reducing structural uncertainty, we now consider several interpretation rules applied to several data sets of increasing density extracted from the reference model. The knowledge of the reference model enables to determine whether the reference association can be retrieved, and to study the influence of chosen geological rules and algorithm parameters on the quality of the generated interpretations.

The multi-scenario association strategy was applied on fault evidence extracted along 3, 4, 5, and 6 cross-sections, using a set of geological rules consistent with the reference model. The distances between two cross-sections are given Table 1 Because such an ideal case is unrealistic in actual sparse data settings, we delete and modify some of the rules to test how the rule choices impact structural interpretation.

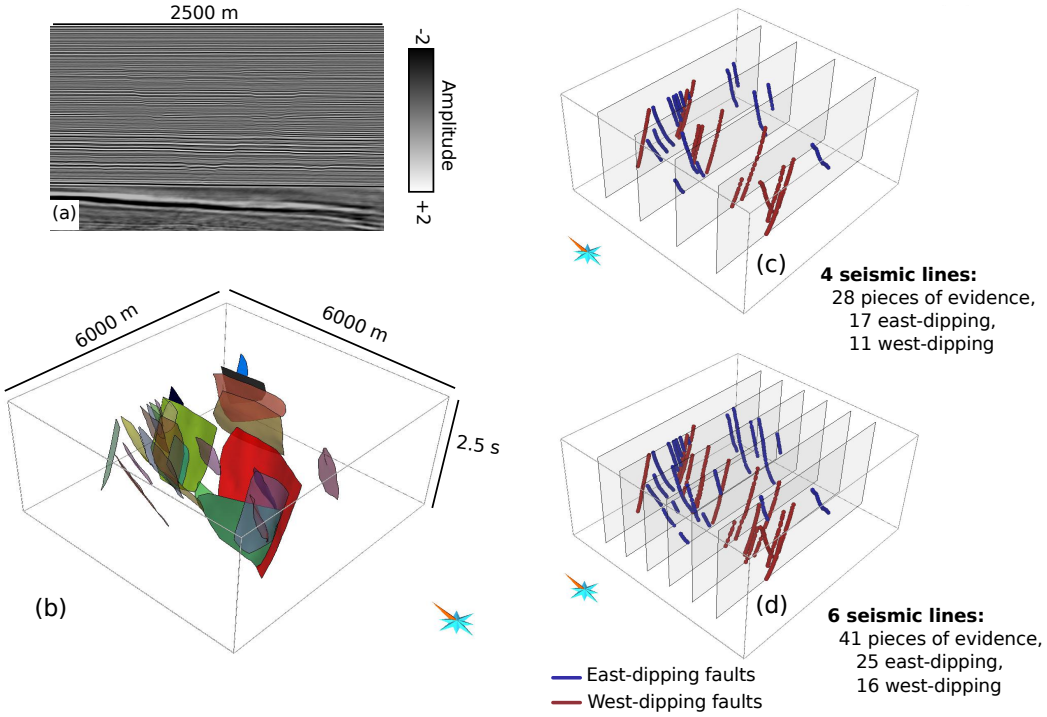

Figure 5. Reference structural model located in the Santos Basin, offshore Brazil. (a) Available reflection seismic data (courtesy of PGS). (b) Reference fault network. (c, d) Generated interpreted synthetic parallel two-dimensional seismic lines. An interactive three-dimensional viewer is available here: `gabrielgodefroy.github.io/StochasticInterpData/Fig5/Fig5.html`

Table 2. Numerical values used in the association rules.

Fault	Distance		Strike			
families	Minimum	Maximum	Minimum	Maximum	Average	Tolerance
Family 1	0 km	3.6 km	$N330$	$N015$	$N352.5$	± 22.5
Family 2	0 km	3.6 km	$N145$	$N195$	$N170$	± 25

Table 3. Number of pieces of fault evidences, corresponding simulation times and Bell number for different number of synthetic seismic lines. Simulations were performed using all rules described in Section 3.1. Simulations were carried out on a PC with an Intel Xeon CPU E5-2650 v3 @ 2.30GHz with 64GB of RAM; the code is not parallelized.

Number of synthetic seismic lines	Number of pieces of evidences...	... in fault family 1	... in fault family 2	Bell numbers	Time to simulate 5.10^7 realizations
3	25	16	9	$B_{25} = 4,6.10^{18}$	03h49m
4	28	17	11	$B_{28} = 6,1.10^{21}$	03h51m
5	35	22	13	$B_{35} = 2,8.10^{29}$	05h30m
6	41	25	16	$B_{41} = 2,3.10^{36}$	06h54m

In the considered data set, faults have approximately a north/south strike and can be grouped into two fault families: east- and west-dipping faults. Two fault family rules are defined based on the dip direction. As seismic lines are oriented east/west, the slope of fault interpretations completely determines the family, so there is no uncertainty about which family each piece of evidence belongs to. To evaluate the likelihood of associating two fault traces, we first use an association rule that restricts the strike of the generated faults to be between $N330$ and $N015$ for the first family, and between $N145$ and $N195$ for the second. Additionally, a uniform association distance rule is created using the largest fault extension observed in the reference model (3.6 km). The numerical values and the mathematical expressions defining these rules are given respectively in Table 2 and Appendix 6.1.

Before applying the simulation algorithm described in Section 2.3, we consider each association rule separately to assess the impact of conceptual information on the structure of the possibility graph (Figure 6). As expected, these restrictive rules decrease the number of edges in $\mathbb{G}_{\varphi}^{\mathbf{all}}$, hence the number of possible association scenarios for each family (see Section 2.2). In the interpreted area of interest, faults do not intersect each other, so intersections are also forbidden during the simulations. In spite of these rules, going from 4 to 6 seismic sections significantly increases both the number of graph nodes (from 28 to 41, see Table 3 for details) and graph edges (from 378 to 820), making it more difficult to explore the search space or to find the optimal fault configuration.

3.2 Sensitivity to scale parameters

The simulation process is parameterized by a scalar value α_{draw} and by a probability density function P_{seg}, which both relate to the fault size and impact the number of simulated fault surfaces. Figure 7 exhibits statistics on the number of simulated faults, while modifying these two parameters. Statistics are computed over 5.10^5 realizations,

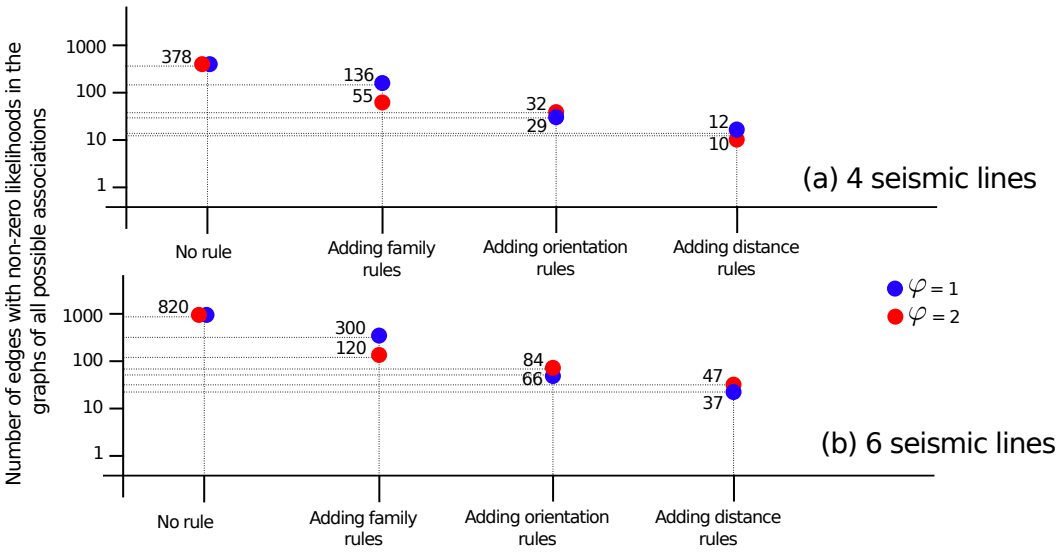

Figure 6. Number of edges per fault family (φ) in the graphs of all possible associations ($\mathbb{G}_{\varphi}^{\mathbf{all}}$) for evidence extracted along (a) 4 seismic lines, and (b) 6 seismic lines. The integration of geological rules (Appendix 6.1) reduces the density of the graphs of all possible associations $\mathbb{G}_{\varphi}^{\mathbf{all}}$. The possibility graphs can be interactively visualized here: `gabrielgodefroy.github.io/StochasticInterpData/Fig6/html/Fig6.html`

with pieces of fault evidence extracted from the Santos Basin model, along 4 and 6 virtual cross-sections. All of the rules described in Section 3.1 are used for these experiments.

The probability density function P_{seg} used to downscale a fault into several segments (Figure 3) clearly influences the mean number of simulated faults (Figure $7a_2, b_2$). As expected, the use of a linearly increasing density function leads to the simulation of more faults as compared to the decreasing function. When the number of fault observations increases, this trend becomes significant whereas the variability over the total set of realizations increases. For applications which seek to preferentially generate parsimonious scenarios in terms of number of faults, the choice of a decreasing law seems appropriate. In general, however, it seems more relevant to explore the search space, so we will choose the uniform law for P_{seg} from now on, as it almost spans the same extreme number of faults as with the increasing or decreasing laws.

The scalar α_{draw} defines the likelihood that major structures (containing more fault data) are selected earlier during the simulation (Equation 3 and step 3.2 in Figure 2). As expected, a negative or a low α_{draw} increases the number of generated fault structures. The mild decrease of this number when α_{draw} is larger than 1 suggests that the other factors tend to naturally limit the appearance of very large fault objects which would gather many fault evidences. This emerging behavior is qualitatively consistent with highly skewed distributions observed for fracture size distributions (Bonnet et al., 2001). In terms of range, choosing $\alpha_{draw} = 2$ approximately spans the same minimum and maximum number of faults as generated with other values, so we will keep a value of 2 in future experiments.

3.3 Evolution of the number of possible scenarios

The proposed sampling method may generate the same fault scenario several times. To assess whether the sampler has converged, a common strategy consists in generating models until the number of *distinct* scenarios stabilizes (Pakyuz-Charrier et al., 2019; Thiele et al., 2016). For this, we use the metric $N_{diff}(l, m)$ which counts the number of differences between any two realizations $\mathbb{G}^{\mathbf{asso}}{}_l$ and $\mathbb{G}^{\mathbf{asso}}{}_m$. N_{diff} is defined as a special case of graph edit distance (Sanfeliu & Fu, 1983), in which the only edit operations are edge insertion and deletion:

$$N_{diff}(l, m) = \sum_{\mathbb{e} \in \mathsf{edges}} d_{l,m}(\mathbb{e}) \tag{4}$$

where

$$d_{l,m}(\mathbb{e}) = \begin{cases} 0 & \text{if the edge } \mathbb{e} \text{ is either present or missing in both } \mathbb{G}^{\mathbf{asso}}{}_l \text{ and } \mathbb{G}^{\mathbf{asso}}{}_m, \\ 1 & \text{if not.} \end{cases} \tag{5}$$

For computational reasons, 5.10^7 realizations were simulated from the fault interpretations extracted from 3, 4, 5, and 6 virtual seismic lines, using all the previously described rules (Figure 8.a). Simulations run in 3 to 7 hours (see Table 3 for details). At the beginning of the simulation, the sampling algorithm shows a near-optimal exploration efficiency as it generates only different realizations, whatever the data density.

For the case with 3 seismic lines, the plateau is not yet fully reached but for the case with 4 seismic lines, a plateau of 6072 distinct realizations is reached after 3.10^6 realizations. In both cases, the reference association is found 2026 times and 3164 times for 3 and 4 seismic lines, respectively. This can be explained by the different information content carried by these data sets (see Figure 6 of the supplementary material). When simulating from 5 and 6 seismic lines (35 and 41 fault data, respectively), the numbers

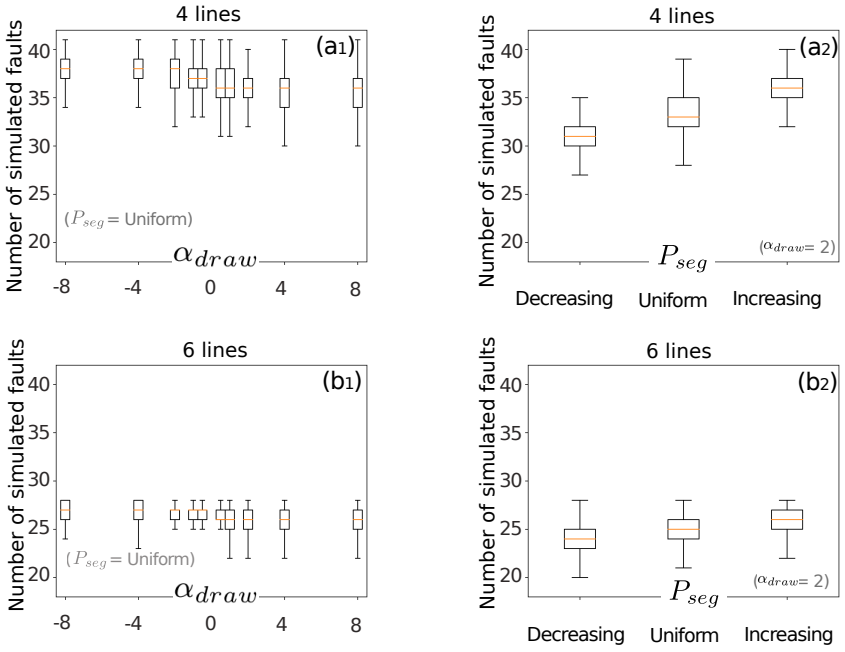

Figure 7. Sensitivity of the number of simulated faults to the parameter α_{draw} (a_1, b_1) and to the probability density function (a_2, b_2) used while drawing the number of fault segments P_{seg}. Statistics computed over 5.10^5 realizations for the cases with 4 (a_1, a_2) and 6 (b_1, b_2) seismic lines.

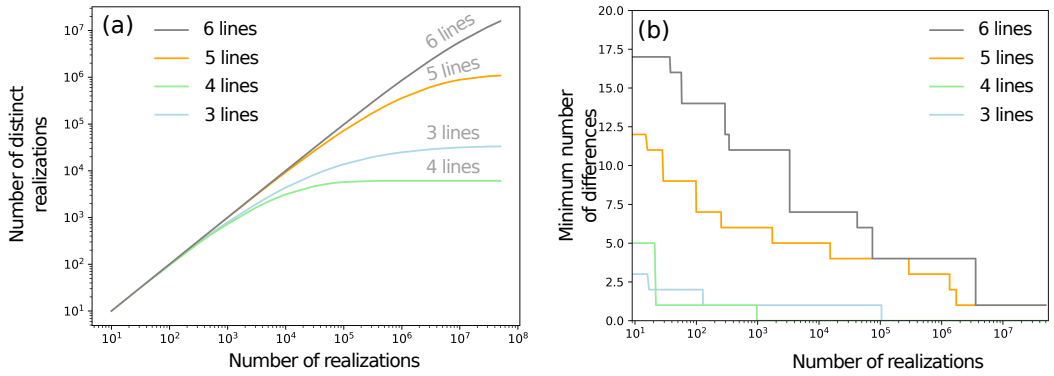

Figure 8. (a) Number of distinct association scenarios obtained from 5.10^7 realizations from 3, 4, 5, and 6 seismic lines. A plateau is not reached for the case with 5 and 6 seismic lines, highlighting the very large computational complexity of the problem. (b) Minimum number of differences to the reference found over the first realizations.

of distinct scenarios is still significantly increasing after 5.10^7 realizations and the reference association is not found. In both cases, the best scenario produced has a number of differences N_{diff} equal to 1 (Figure 8.b).

This numerical experiment shows the difficulty of retrieving the reference association when the number of pieces of fault evidence is high, even if the chosen rules are restrictive and consistent. Indeed, as discussed in Section 2.2, the combinatorial complexity increases in a non-polynomial way with the number of nodes. The proposed formalism is thus favorable when relatively few pieces of fault evidence are available, and when the association rules strongly constrain the solution space. This is consistent with expectation that more data brings new knowledge and thus reduces the uncertainties. However, the experiment shows that this information effect can be significantly counterbalanced by the difficulty to explore a larger search space, as also observed by Edwards et al. (2018) for well correlation.

3.4 Influence of the chosen geological rules on simulation results

3.4.1 Impact of the number of rules

We tested the impact of the chosen numerical rules by successively running simulations with an increasing number of rules (orientation rule, distance between pieces of fault evidence, and forbidding fault intersections). 5.10^5 realizations were generated from digitized fault evidence extracted along the 3, 4, 5, and 6 seismic lines.

To analyze these results, we now consider the number of differences $N_{diff}(l, ref)$ between each simulated association $\mathbb{G}^{\mathbf{asso}^l}$ and the reference association $\mathbb{G}^{\mathbf{asso}}_{ref}$ interpreted from the full 3D seismic data set. When the simulations are run with more rules (Figure $9.a_1 - a_4$), the minimum, mean, and maximum number of differences $N_{diff}(l, ref)$ consistently decrease. Moreover, we observe that rules interact with the data density on

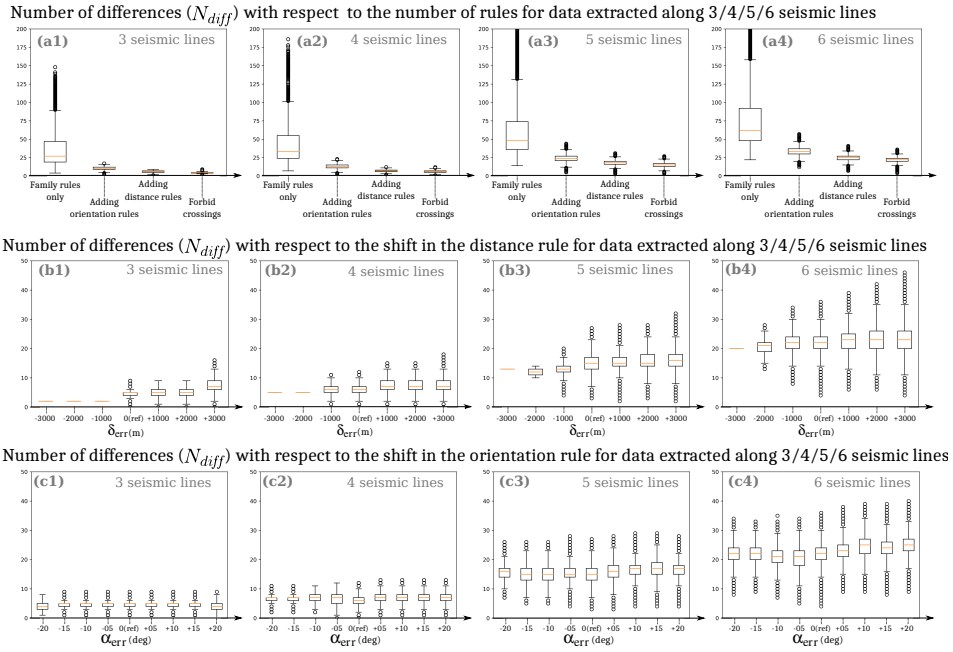

Figure 9. Box plots showing the minimum, mean and maximum number of differences (N_{diff}) between the simulated association graphs and the reference one. Graphs computed for sparse data extracted from 3 (a_1 – c_1) to 6 (a_4 – c_4) seismic lines. (a_1 – a_4) The integration of more geological rules reduces the range of possibilities, corresponding to lower density for the graphs of all geologically meaningful associations $\mathbb{G}_{\varphi}^{\mathbf{all}}$. Falsification of the distance rule (b_1 – b_4) and of the orientation rule ($c_1 - c_4$). Statistics computed over 5.10^5 realizations.

two respects. First, considering a single rule in sparse data settings (cases with 3 or 4 sections) yields realizations closer to the reference than considering more informative rules in denser data settings (cases with 5 or more sections). This can be explained by the non-convergence of the sampler for 5 and 6 sections, as shown in Figure 8.a. Second, for a given set of rules, the absolute number of differences from the reference increases with the number of data. This is a direct effect of the increasing complexity of the search space, and may also be explained by the non-convergence of the sampler with 5.10^7 realizations for more than 5 seismic lines (Figure 9.a_4).

It would be interesting to weight these distributions by a relative likelihood for each particular scenario using the correlation rules. If appropriately chosen, the rules should then give a larger weight to the scenarios closer to the reference. However, computing such a relative likelihood faces again a normalization challenge, as the number of graph edges is generally different for each realization.

3.4.2 Deliberately selecting biased rules

In practical geological studies, it would be difficult to come up with appropriate parameters for the association rules. Therefore, we tested the impact of choosing erroneous geological concepts during structural interpretation: the orientations defining the associations rules were shifted by an angle α_{err} and the distance max_{dist} defining the distance association rule was offset by δ_{err}. The mathematical expressions for the falsified rules are given in Appendix 6.1.

We study the mean number of differences to the reference association (over 5.10^5 realizations) according to these inappropriate choices (Figure 9.b,c). Strongly biased rules make it impossible to retrieve the reference association from fault evidence sampled along 3, 4, 5 or 6 seismic lines (Figure 9.b_1, b_2, c_1, c_2, b_3, b_4 and c_3, c_4, respectively). When simulating interpretation scenarios from data extracted along 5 or 6 seismic sections, the reference scenario is never retrieved.

In the case of the distance rule, if δ_{err} is negative, no association is allowed, yielding a collapse of the ensemble of associations. Such a collapse clearly highlights an inconsistency between the rules and the spacing of the synthetic data. On the other hand, if the distance rule is more permissive than the reference one (i.e., δ_{err} is positive), then the minimum, mean, and maximum numbers of error increase for all number of seismic lines.

The effect of changing the orientation rule is not as dramatic, but for the cases with 5 and 6 seismic lines, the deviation from the reference rules leads to a slight increase of the mean numbers of error.

4 Discussion and ways forward

4.1 On objectivity and uncertainty

The proposed graph-based sampling method is a new framework to rapidly and automatically explore fault network uncertainties by generating stochastic fault scenarios from sparse observations. As compared to classical fault interpretation approaches where experts associate the pieces of evidence based on their prior knowledge, our approach forces the interpreter to explicitly formulate elementary association rules, which are aggregated by a stochastic algorithm. The promise of this work is to make interpretation an objective, unbiased and reproducible process. However, the geological interpretation of subsurface data is precisely about adding some conceptual knowledge to the data, which

cannot be fully objective and will always depend on the current state of knowledge and experience of an interpreter or on some model assumptions (Bond et al., 2007; Chamberlin, 1890; Frodeman, 1995; Wellmann & Caumon, 2018). In this paper, we used relatively general rules to define fault data association likelihoods, but the order by which we processed and combined them is certainly subjective and driven in part by mathematical and algorithmic convenience, so we do not claim it to be fully objective. Nonetheless, as compared to classical expert-based interpretation, we see the general approach proposed in this paper as a step towards making the interpretation process more transparent and reproducible using a probabilistic way of expressing and combining geological concepts.

Another major difference between this approach and the expert-based method is the intrinsic ability of the former to generate several scenarios, whereas most of the latter tend to end up with one deterministic solution. A reason is that interpretation exercises are taught as a deterministic activity in the vast majority of university courses: the general expectation, in surface or subsurface mapping, is to produce only the most likely scenario or model. This is shown even in experiments assessing the interpretation uncertainty, which ask a set of geoscientists to produce one interpretation each (Bond et al., 2007; Bond, 2015; Schaaf & Bond, 2019). Cognitive biases also explain the difficulty of one to work with multiple hypotheses (Chamberlin, 1890; Wilson et al., 2019), which is a possible explanation for interpretation bias (Bond et al., 2007). The advent of computer-based methods makes it easier to explore aleatory uncertainties by perturbing a reference model (see Wellmann & Caumon, 2018, and references therein), but addressing epistemic uncertainties is more challenging as it requires to formalise the geological concepts. The method proposed in this paper clearly belongs to this latter class of methods.

4.2 On graphs for structural uncertainty assessment

We see the graph-based method proposed in this paper as a possible way to complement or generalize previous structural uncertainty evaluation approaches:

- It is a parsimonious approach which starts from existing observations. As such, it follows the same philosophy as data perturbation strategies, which consider that spatial observations have uncertain location and/or orientation (Lindsay et al., 2012; Pakyuz-Charrier et al., 2018; Wellmann et al., 2010). However, a major conceptual difference exists. Indeed, even though the topology of the geological model may change by sampling data orientation only, fault data must be associated a priori with a particular fault surface. In contrast, our approach starts without any particular assumption about how to associate incomplete fault observations together. It can be seen as a way to randomly change the data labels, and can be used before sampling from orientation or location distributions associated with incomplete observations. Data uncertainty can also be integrated in the graph-based framework.
- Another class of methods to address structural uncertainty is to proceed by geometric perturbation techniques of an existing structural model (Holden et al., 2003; Lecour et al., 2001; Røe et al., 2014). These methods keep the fault connectivity of the initial structural model constant, but may change the connectivity of rock units on either sides of faults by changing the fault throw. In this paper, we tried to reduce the risk of bias by focusing on large-scale fault topological changes, starting from the observations rather than from an initial fault network interpretation. Note, however, that all data known to belong to the same fault surface can be associated in a deterministic way in the proposed graph-based method.
- Approaches addressing topological fault network uncertainty have been proposed before, using mainly data-driven iterative simulation methods (Cherpeau et al.,

2010a; Cherpeau & Caumon, 2015; Julio et al., 2015b) or object simulation based on stochastic point processes (Aydin & Caers, 2017; Cherpeau et al., 2010b; Hollund et al., 2002; Munthe et al., 1994). All data-driven approaches, including the method presented herein, can be seen as an efficient way to honor observations, which is a notably difficult and time-consuming process when the spacing between observations is smaller than the size of the simulated objects. Data-driven fault simulations are also parsimonious as they only focus on explaining observations, but they can significantly under-estimate the number of faults in a given domain. For example, the Santos case study clearly shows that the number of simulated faults decreases when less data is used for the same area of interest (Figure 7). Therefore, we firmly believe that a stochastic point process should ultimately complement the proposed approach to simulate faults that are not directly supported by observations (Aydin & Caers, 2017; Bonneau et al., 2016; Cherpeau et al., 2010b; Davy et al., 2013; Holden et al., 2003; Munthe et al., 1994; Stoyan & Gloaguen, 2011). Such a process would generate new nodes in the graph $\mathbb{G}^{\mathbf{asso}}$. A particular challenge would be to choose an appropriate point process and to come up with a sound parameter inference strategy for the stochastic process. This includes avoiding collisions between simulated faults and existing cross-sections or boreholes where no fault has been observed. Another line of progress in the graph-based method concerns the management fault branch lines. Indeed, even though the chosen reference data set (Figure 5) is free of fault branchings, most faults branch or interact together during their growth (Nicol et al., 2020). A second oriented graph could be considered and updated during the simulation algorithm to represent how faults branch in the fault network. The simulation process should account for the chronology of the development of the successive fault families to preserve the spatial dependency of fault geometry, hierarchy and the fault abutting relationship (as in Aydin & Caers, 2017; Cherpeau et al., 2010b). This would imply updating the association likelihoods (calculated at step 2.1 in Fig. 2) after each stochastic step of the simulation algorithm (step 3.3 of Fig. 2).

Unlike previous iterative methods (Aydin & Caers, 2017; Cherpeau et al., 2010a; Cherpeau & Caumon, 2015), the potential major fault structures are processed in the early steps of our algorithm thanks to the maximal clique detection. Assuming that largest faults are most likely to correspond to many graph nodes, this reproduces a classical interpretation process whereby geologists focus on largest structures before focusing on smaller objects (e.g., Lines & Newrick, 2004). Therefore, we believe that the graph-based approach more effectively explores the search space than previous iterative methods, which tend to proceed by local propagation of information. The proposed clique subdivision is another way to formalize fault downscaling approaches (Julio et al., 2015b; Manighetti et al., 2015). It would be interesting, nonetheless, to quantitatively study how much the proposed strategy affects the sampled model space as compared to previous iterative methods.

4.3 Are the produced interpretations "geologically realistic"?

The proposed graph-based method enables the interactive definition of new rules according to a specific geological context. Overall, we only tested relatively simple geological rules in this paper in order to assess the consistency of the sampling algorithm. The method allows for formulating additional rules to improve the consistency of the obtained results and reduce the search space, for example: to choose fault surface orientations from analog data sets (Aydin & Caers, 2017), to account for fault curvature and lateral extension, and an estimation of the fault slip (Cherpeau & Caumon, 2015; Røe et al., 2014), to evaluate fault segmentation (Julio et al., 2015a; Manighetti et al., 2015; Manzocchi et al., 2019).

Such formalizations of geological knowledge as additional numerical rules clearly call for more studies to come up with appropriate choice of rules and parameters. In this paper, we started by choosing an ideal case where the parameters of simple rules were calibrated directly on a reference model. We acknowledge that this is never the case in practice where no reference model exists. Tests made in Section 3.4.2 suggest that, when rule parameters are chosen inappropriately, the simulated models can show significant bias, and we can expect that this observation would also hold for more complex rules. Therefore, further studies are needed to help geoscientists to define the numerical interpretation rules to be used in a particular geological context, how to choose their parameters and how to combine them. This could rely on outcrop or subsurface analog data bases, analog laboratory models, or process-based numerical models, or on an inference process applied directly to the data at hand. Machine learning could also come into play in this process, either by inferring rule parameters or a posteriori assessing the likelihood of the various realizations produced by the sampling method. Training for these approaches could be achieved on multiple manual interpretations (e.g., Schaaf & Bond, 2019) or on processed synthetic models (Wu et al., 2019).

The graph-based sampler, when appropriately parameterized, could, in principle, (1) lead to a more objective characterization of structural uncertainty as compared to manual interpretation and (2) help reducing cognitive biases (Wilson et al., 2019). However, an automatic method such as the graph-based sampling proposed in this paper has no guarantee to produce the same results as several interpretations made by several experts. One reason is that experts can be biased, but this could be addressed in principle by selecting a sufficiently large number of experts. Another, more serious reason, is that the sampling method is likely to miss some important aspects of geological interpretation. On this regard, we see two main avenues for improvement:

- First, the methodology does not completely automate the three-dimensional structural modeling, which makes it difficult to assess the likelihood of the generated fault networks using advanced structural analyzes such as global displacement analysis (Freeman et al., 2010) or structural restoration (Gratier & Guillier, 1993). For this, faults geometries should be modeled using explicit surfaces (Lecour et al., 2001; Røe et al., 2014) or implicit surfaces (Aydin & Caers, 2017; Cherpeau et al., 2010b). Then, the geological formations affected by the fault network should be modeled as done for example by Cherpeau and Caumon (2015); Godefroy et al. (2017); Laurent et al. (2013). The fault geometries need to be simulated while accounting for theoretical tip-line geometries (e.g., Barnett et al., 1987) and theoretical scaling laws (e.g., Torabi & Berg, 2011). Generating such geometries would be useful to assess the impact of fault network uncertainty on resource assessment (Richards et al., 2015), to incorporate this source of uncertainty in geophysical inverse problems (Giraud et al., 2019; Ragon et al., 2018), or to formulate the "geological realism" problem as an Bayesian inference problem (de la Varga & Wellmann, 2016).
- Second, the graph formalism at this stage only considers pairwise associations but does not use the likelihood of associating several nodes at once. For example, it could be likely to associate the pieces of evidence A and B, B and C, and A and C independently, but very unlikely to associate A, B and C altogether. This calls for the definition of multi-point, higher-order statistical rules which apply to graph cliques. For example, one could consider the throw distribution along fault strike (as in Cherpeau & Caumon, 2015; Freeman et al., 1990) or statistical relationships between observed separations and fault size (e.g., Gillespie et al., 1992; Torabi & Berg, 2011). The association likelihoods could also be updated during the graph-based sampling algorithm to account for the fact that fault-fault intersections at large scale are unlikely but are not necessarily impossible (Schneeberger et al., 2017).

To bridge the gap between automatic interpretation methods such as proposed in this paper and classical expert-based techniques, a possible avenue could be to share and interactively render three-dimensional objects on a web server to quantitatively study how a large number of geologists interpret available data. This was recently proposed by Schaaf and Bond (2019) using three-dimensional subsurface models created by a class of students. Using numerical interpretation tools could further enable to record the interpreter strategies, and for example, to detect which geological structures geologists interpret first.

4.4 Inverse problem and clustering of structural interpretations

Stochastic structural modeling enables to generate large numbers of alternative scenarios (several millions in this work) which can be used as prior information in subsurface inverse problems (see Wellmann and Caumon (2018) and references therein). However, the automatic generation of a three-dimensional meshed model for each interpretation is currently impossible. The computational times of focal mechanism inversion, flow simulation, or seismic forward modeling are often incompatible with more than hundreds or maybe thousands of models. Furthermore, for a human being, it seems difficult to work with more than a few alternative scenarios deemed representative of the uncertainties. An effective way to address this problem is to use model clustering in model space (e.g., Suzuki et al., 2008) or in data space (i.e., based on the similarity between their forward response, see for example Scheidt et al., 2018; Irakarama et al., 2019). A challenge, in both cases, comes from the redundancy of models sampled by a particular stochastic methods: indeed, simulation methods tend to generate many similar models in a priori likely regions of the search space. This redundancy is needed if the models also have a large posterior probability, but it can raise efficiency problems when the Bayesian updating is strong. Also, the above methods tend to search for model clusters *after* the sampling stage, which is not optimal.

The graph-based sampler described in this paper opens some avenues to make progress in this area. Indeed, maximal cliques are detected and processed sequentially within the sampling algorithm. Therefore, a hierarchical clustering of structural scenarios could be generated by applying the method in a recursive manner. A possible and simplified outline of such a hierarchical sampling reads:

1. Define the starting possibility graph $\mathbb{G}_0^{\mathbf{all}} \leftarrow \mathbb{G}^{\mathbf{all}}$ and the starting index $h \leftarrow 0$
2. Find the maximal cliques of $\mathbb{G}_h^{\mathbf{all}}$
3. Generate N_h scenarios by sampling a possible fault from the maximal cliques. Denote as $\mathbb{V}_{n_h}$, $n_h = 1, \ldots, N_h$ the set of graph vertices corresponding to that clique.
4. For each scenario $n_h = 1, \ldots, N_h$:
   (a) Increment the hierarchical level $h \leftarrow h + 1$
   (b) Update the current possibility graph: $\mathbb{G}_h^{\mathbf{all}} \leftarrow \mathbb{G}_{h-1}^{\mathbf{all}} \setminus \mathbb{V}_{n_h}$
   (c) If $\mathbb{G}_h^{\mathbf{all}}$ still has vertices, go to Step 2, otherwise terminate.

5 Conclusions

The proposed graph-based framework helps interpreting alternative fault scenarios to account for the uncertainty arising while considering sparse fault sample. Prior geological knowledge is formalized using numerical geological rules, enforcing the geological consistency of the interpretation choices. The mathematical format of the rules eases the communication of the geological concepts used during the interpretation as compared to manual interpretation approaches, and makes the structural interpretation process reproducible.

Each scenario is represented by a graph. The automatic interpretation framework relies on maximal cliques, i.e., major possible structures in the graphs of all possible associations. This strategy mimics the behavior of an interpreter who would start by the structures explained by a large amount of evidence. The use of a light graph data structure, as compared with a full three-dimensional model, leads to a fast simulation process. This rapidity allows to perform sensitivity studies on the numerical rules and simulation parameters using sparse data extracted from a reference model.

The presented numerical experiments illustrate the difficulty in retrieving the correct association scenario from sparse data. Even if interpretation rules reduce the number of scenarios, it seems highly unlikely that a single interpretation is correct. This reminds us that, when working with subsurface data, uncertainty is the norm and not the exception (Frodeman, 1995). These experiments also confirm that the simultaneous use of several coherent geological rules reduces the number of distinct simulated scenarios. The simulated models are closest (on average) to the reference model and rule falsification decreases the likelihood to find a scenario close to the reference one. These experiments formally show the importance of the prior geological knowledge during structural interpretation.

We also advocate for making geologists aware of structural uncertainties in the early stages of their training during geological education (Chamberlin, 1890). Formalizing explicitly the interpretation concepts should ease their communication and limit interpretation biases.

Acknowledgments

This work was performed in the frame of the RING project (http://ring.georessources.univ-lorraine.fr/) at Université de Lorraine. We would like to thank for their support the industrial and academic sponsors of the RING-GOCAD Consortium managed by ASGA. Software corresponding to this paper is available to sponsors in the RING software package FaultMod2. We also acknowledge Paradigm for the SKUA-GOCAD Software and API. The authors are grateful to PGS Investigação Petrolífera Limitada and to Chris A.L. Jackson for providing the Santos Basin reflection seismic data. Readers can access the reference structural model and the generated synthetic cross-sections using the following DOI: https://doi.org/10.17605/OSF.IO/MP97W.

6 Appendices

6.1 Rules expression

We give here the numerical formulas and values used to compute the association likelihoods $L_{\varphi}^{\mathbf{all}}(\mathbb{v}_i \leftrightarrow \mathbb{v}_j)$ in the case study presented in Section 3.

No rule If no prior geological knowledge is used, all the associations are assumed equally likely and

$$L_{\varphi_i}^{\mathbf{all}}(\mathbb{v}_i \leftrightarrow \mathbb{v}_j) = 1$$

for $i \in \{1, 2\}$.

Family rule only If only family rules are used, then $R_{\varphi}^{\mathbf{fam}}(\mathbb{v}_i) = 1$ and

$$L_{\varphi_i}^{\mathbf{all}}(\mathbb{v}_i \leftrightarrow \mathbb{v}_j) = R_{\varphi_i}^{\mathbf{fam}}(\mathbb{v}_i).$$

In this Santos Basin case study, the family rules rely on the dip orientation of the digitized fault evidence, and

$$R^{\mathbf{fam}}_{\varphi_1}(\mathbb{v}_i) = \begin{cases} 1, & \text{if the piece of fault evidence } \mathbb{v}_i \text{ is dipping toward the West, and} \\ 0, & \text{otherwise.} \end{cases}$$

As there is no uncertainty on which family the pieces of evidence belong to, the rule for the family φ_2 can be computed from the one for φ_1: $R^{\mathbf{fam}}_{\varphi_2}(\mathbb{v}_i) = 1 - R^{\mathbf{fam}}_{\varphi_1}(\mathbb{v}_i)$.

Orientation rules The orientation computed between two pieces of evidence is accounted using a rule and combined with the previously defined family rules using

$$L^{\mathbf{all}}_{\varphi}(\mathbb{v}_i \leftrightarrow \mathbb{v}_j) = R^{\mathbf{fam}}_{\varphi}(\mathbb{v}_i)\, R^{\mathbf{fam}}_{\varphi}(\mathbb{v}_j)\, R^{\mathbf{assoc}}_{\varphi}(\mathbb{v}_i \leftrightarrow \mathbb{v}_j),$$

with $R^{\mathbf{assoc}}_{\varphi}(\mathbb{v}_i \leftrightarrow \mathbb{v}_j) = R^{orient}_{\varphi}$ being a discrete association rule:

$$R^{orient}_{\varphi_i} = \begin{cases} 1, & \text{if the strike orientation between } \mathbb{v}_i \text{ and } \mathbb{v}_j \text{ is between } min^{strike}_{\varphi_i} \text{ and } max^{strike}_{\varphi_i}, \\ 0, & \text{otherwise,} \end{cases}$$

with $min^{strike}_{\varphi_1} = 330$, $max^{strike}_{\varphi_1} = 15$, $min^{strike}_{\varphi_2} = 145$, and $max^{strike}_{\varphi_2} = 195$.

All rules In this last case, a distance rule is also taken into account. The distance association likelihood is defined

$$R^{dist}_{\varphi}(\mathbb{v}_i \leftrightarrow \mathbb{v}_j) = max(1 - dist(\mathbb{v}_i \leftrightarrow \mathbb{v}_j)/max_{dist}, 0),$$

with $max_{dist} = 3600$ being the dimension (in meter) of the longest fault observed in the area of interest. This association rule is combined with the orientation rule:

$$R^{\mathbf{assoc}}_{\varphi}(\mathbb{v}_i \leftrightarrow \mathbb{v}_j) = R^{dist}_{\varphi}(\mathbb{v}_i \leftrightarrow \mathbb{v}_j) R^{orient}_{\varphi}(\mathbb{v}_i \leftrightarrow \mathbb{v}_j).$$

Rule falsifications In Section 3.4.2, the numerical values used for the orientation and distance rules are falsified to become:

$$\begin{cases} min^{strike}_{\varphi_1} = 330 + \alpha_{err}, \\ max^{strike}_{\varphi_1} = 15 + \alpha_{err}, \\ min^{strike}_{\varphi_2} = 145 + \alpha_{err}, \\ max^{strike}_{\varphi_2} = 195 + \alpha_{err}, \text{and} \\ max_{dist} = 3600 + \delta_{err}. \end{cases}$$

References

Anquez, P., Pellerin, J., Irakarama, M., Cupillard, P., Lévy, B., & Caumon, G. (2019, January). Automatic correction and simplification of geological maps and cross-sections for numerical simulations. *Comptes Rendus Geoscience*, *351*, 48-58. doi: 10.1016/j.crte.2018.12.001

Aydin, O., & Caers, J. K. (2017). Quantifying structural uncertainty on fault networks using a marked point process within a Bayesian framework. *Tectonophysics*, *712*, 101–124. doi: 10.1016/j.tecto.2017.04.027

Barnett, J. A., Mortimer, J., Rippon, J. H., Walsh, J. J., & Watterson, J. (1987). Displacement geometry in the volume containing a single normal fault. *AAPG Bulletin*, *71*(8), 925–937.

Bond, C. (2015). Uncertainty in structural interpretation: Lessons to be learnt. *Journal of Structural Geology*, *74*, 185–200. doi: 10.1016/j.jsg.2015.03.003

Bond, C., Gibbs, A., Shipton, Z., & Jones, S. (2007). What do you think this is? "Conceptual uncertainty"in geoscience interpretation. *GSA Today*, *17*(11), 4. doi: 10.1130/GSAT01711A.1

Bonneau, F., Caumon, G., & Renard, P. (2016). Impact of a stochastic sequential initiation of fractures on the spatial correlations and connectivity of discrete fracture networks. *Journal of Geophysical Research: Solid Earth*, *121*(8), 5641–5658. doi: 10.1002/2015JB012451

Bonnet, E., Bour, O., Odling, N. E., Davy, P., Main, I., Cowie, P., & Berkowitz, B. (2001). Scaling of fracture systems in geological media. *Reviews of geophysics*, *39*(3), 347-383.

Bron, C., & Kerbosch, J. (1973). Algorithm 457: finding all cliques of an undirected graph. *Communications of the ACM*, *16*(9), 575–577. doi: 10.1145/362342.362367

Caumon, G. (2010). Towards stochastic time-varying geological modeling. *Mathematical Geosciences*, *42*(5), 555-569.

Chamberlin, T. C. (1890). The method of multiple working hypotheses. *Science*, *15*(366), 92–96.

Cherpeau, N., & Caumon, G. (2015). Stochastic structural modelling in sparse data situations. *Petroleum Geoscience*, *21*(4), 233–247. doi: 10.1144/petgeo2013-030

Cherpeau, N., Caumon, G., Caers, J., & Lévy, B. (2012). Method for stochastic inverse modeling of fault geometry and connectivity using flow data. *Mathematical Geosciences*, *44*(2), 147–168. doi: 10.1007/s11004-012-9389-2

Cherpeau, N., Caumon, G., & Lévy, B. (2010a). Stochastic simulation of fault networks from 2D seismic lines. In *SEG Expanded Abstracts* (Vol. 29, pp. 2366–2370). doi: 10.1190/1.3513325

Cherpeau, N., Caumon, G., & Lévy, B. (2010b). Stochastic simulations of fault networks in 3d structural modeling. *Comptes Rendus Géoscience*, *342*(9), 687–694. doi: 10.1016/j.crte.2010.04.008

Davy, P., Le Goc, R., & Darcel, C. (2013). A model of fracture nucleation, growth and arrest, and consequences for fracture density and scaling. *Journal of Geophysical Research: Solid Earth*, *118*(4), 1393–1407. doi: 10.1002/jgrb.50120

de la Varga, M., & Wellmann, J. F. (2016, August). Structural geologic modeling as an inference problem: A Bayesian perspective. *Interpretation*, *4*(3), SM1-SM16. doi: 10.1190/INT-2015-0188.1

Edwards, J., Lallier, F., Caumon, G., & Carpentier, C. (2018). Uncertainty management in stratigraphic well correlation and stratigraphic architectures: A training-based method. *Computers & Geosciences*, *111*, 1–17. doi: 10.1016/j.cageo.2017.10.008

Emerson. (2018). *SKUA-GOCAD.* `https://www.pdgm.com/products/skua-gocad/`.

Ferrill, D. A., Stamatakos, J. A., & Sims, D. (1999). Normal fault corrugation: Implications for growth and seismicity of active normal faults. *Journal of Structural Geology*, *21*(8), 1027–1038. doi: 10.1016/S0191-8141(99)00017-6

Frank, T., Tertois, A.-L., & Mallet, J.-L. (2007, July). 3D-reconstruction of complex geological interfaces from irregularly distributed and noisy point data. *Computers & Geosciences*, *33*(7), 932-943. doi: 10.1016/j.cageo.2006.11.014

Freeman, B., Boult, P. J., Yielding, G., & Menpes, S. (2010). Using empirical geological rules to reduce structural uncertainty in seismic interpretation of faults. *Journal of Structural Geology*, *32*(11), 1668–1676. doi: 10.1016/j.jsg.2009.11.001

Freeman, B., Yielding, G., & Badley, M. (1990). Fault correlation during seismic interpretation. *First Break*, *8*(3), 87–95. doi: 10.3997/1365-2397.1990006

Frodeman, R. (1995). Geological reasoning: Geology as an interpretive and historical

science. *Geological Society of America Bulletin*, *107*(8), 960–968. doi: 10.1130/0016-7606(1995)107⟨0960:GRGAAI⟩2.3.CO;2

Gillespie, P., Walsh, J., & Watterson, J. (1992). Limitations of dimension and displacement data from single faults and the consequences for data analysis and interpretation. *Journal of Structural Geology*, *14*(10), 1157–1172. doi: 10.1016/0191-8141(92)90067-7

Giraud, J., Lindsay, M., Jessell, M., & Ogarko, V. (2019). Towards geologically reasonable lithological classification from integrated geophysical inverse modelling: Methodology and application case. *Solid Earth Discussions*, *2019*, 1–27. doi: 10.5194/se-2019-164

Godefroy, G., Caumon, G., Ford, M., Laurent, G., & Jackson, C. A.-L. (2017). A parametric fault displacement model to introduce kinematic control into modeling faults from sparse data. *Interpretation*, *6*(2), 1–48. doi: 10.1190/int-2017-0059.1

Godefroy, G., Caumon, G., Laurent, G., & Bonneau, F. (2019). Structural interpretation of sparse fault data using graph theory and geological rules. *Mathematical Geosciences*.

Gombert, B., Duputel, Z., Jolivet, R., Doubre, C., Rivera, L., & Simons, M. (2018, February). Revisiting the 1992 Landers earthquake: A Bayesian exploration of co-seismic slip and off-fault damage. *Geophysical Journal International*, *212*(2), 839-852. doi: 10.1093/gji/ggx455

Gratier, J.-P., & Guillier, B. (1993, March). Compatibility constraints on folded and faulted strata and calculation of total displacement using computational restoration (UNFOLD program). *Journal of Structural Geology*, *15*(3-5), 391–402. doi: 10.1016/0191-8141(93)90135-W

Grose, L., Ailleres, L., Laurent, G., Armit, R., & Jessell, M. (2019). Inversion of geological knowledge for fold geometry. *Journal of Structural Geology*, *119*, 1–14. doi: 10.1016/j.jsg.2018.11.010

Grose, L., Laurent, G., Aillères, L., Armit, R., Jessell, M., & Cousin-Dechenaud, T. (2018). Inversion of structural geology data for fold geometry. *Journal of Geophysical Research: Solid Earth*, *123*(8), 6318–6333. doi: doi.org/10.1029/2017JB015177

Henza, A. A., Withjack, M. O., & Schlische, R. W. (2011). How do the properties of a pre-existing normal-fault population influence fault development during a subsequent phase of extension? *Journal of Structural Geology*, *33*(9), 1312–1324. doi: 10.1016/j.jsg.2011.06.010

Holden, L., Mostad, P., Nielsen, B. F., Gjerde, J., Townsend, C., & Ottesen, S. (2003). Stochastic structural modeling. *Mathematical Geology*, *35*(8), 899–914. doi: 10.1023/B:MATG.0000011584.51162.69

Hollund, K., Mostad, P., Nielsen, B. F., Holden, L., Gjerde, J., Contursi, M. G., ... Sverdrup, E. (2002). Havana - a fault modeling tool. *Norwegian Petroleum Society Special Publications*, *11*, 157–171.

Irakarama, M., Cupillard, P., Caumon, G., Sava, P., & Edwards, J. (2019). Appraising structural interpretations using seismic datatheoretical elements. *Geophysics*, *84*(2), N29–N40.

Irving, A., Chavanne, E., Faure, V., Buffet, P., & Barber, E. (2010). An uncertainty modelling workflow for structurally compartmentalized reservoirs. *Geological Society, London, Special Publications*, *347*(1), 283–299.

Jessell, M., Ailleres, L., & de Kemp, E. A. (2010, July). Towards an integrated inversion of geoscientific data: What price of geology? *Tectonophysics*, *490*(3-4), 294-306. doi: 10.1016/j.tecto.2010.05.020

Jessell, M., Aillères, L., De Kemp, E., Lindsay, M., Wellmann, J., Hillier, M., ... Martin, R. (2014). Next generation three-dimensional geologic modeling and inversion. *Economic Geology*, *18*, 261–272.

Julio, C. (2015). *Conditionnement de la modélisation stochastique 3D des réseaux de failles* (Unpublished doctoral dissertation). Universite de Lorraine.

Julio, C., Caumon, G., & Ford, M. (2015a). Impact of the en echelon fault connectivity on reservoir flow simulations. *Interpretation*, *3*(4), SAC23–SAC34. doi: 10.1190/INT-2015-0060.1

Julio, C., Caumon, G., & Ford, M. (2015b). Sampling the uncertainty associated with segmented normal fault interpretation using a stochastic downscaling method. *Tectonophysics*, *639*, 56–67. doi: 10.1016/j.tecto.2014.11.013

Knuth, D. E. (2005). *The Art of Computer Programming, Volume 4: Generating all Combinations and Partitions, Fascicle 3*. Addison-Wesley Professional.

Lallier, F., Antoine, C., Charreau, J., Caumon, G., & Ruiu, J. (2013). Management of ambiguities in magnetostratigraphic correlation. *Earth and Planetary Science Letters*, *371*, 26–36. doi: 10.1016/j.epsl.2013.04.019

Laurent, G., Caumon, G., Bouziat, A., & Jessell, M. (2013, April). A parametric method to model 3D displacements around faults with volumetric vector fields. *Tectonophysics*, *590*, 83–93. doi: 10.1016/j.tecto.2013.01.015

Lecour, M., Cognot, R., Duvinage, I., Thore, P., & Dulac, J.-C. (2001). Modelling of stochastic faults and fault networks in a structural uncertainty study. *Petroleum Geoscience*, *7*(S), S31–S42. doi: 10.1144/petgeo.7.S.S31

Levenshtein, V. I. (1966). Binary codes capable of correcting deletions, insertions, and reversals. In *Soviet physics doklady* (Vol. 10, pp. 707–710).

Lindsay, M. D., Aillères, L., Jessell, M. W., de Kemp, E. A., & Betts, P. G. (2012). Locating and quantifying geological uncertainty in three-dimensional models: Analysis of the Gippsland Basin, southeastern Australia. *Tectonophysics*, *546*, 10–27. doi: 10.1016/j.tecto.2012.04.007

Lines, L. R., & Newrick, R. T. (2004). *Fundamentals of Geophysical Interpretation*. Society of Exploration Geophysicists. doi: 10.1190/1.9781560801726

Mai, P. M., Galis, M., Thingbaijam, K. K. S., Vyas, J. C., & Dunham, E. M. (2017, September). Accounting for Fault Roughness in Pseudo-Dynamic Ground-Motion Simulations. *Pure and Applied Geophysics*, *174*(9), 3419-3450. doi:

10.1007/s00024-017-1536-8

Mallet, J.-L. (1992). Discrete smooth interpolation in geometric modelling. *Computer-aided design*, *24*(4), 178–191. doi: 10.1016/0010-4485(92)90054-E

Manighetti, I., Caulet, C., Barros, L., Perrin, C., Cappa, F., & Gaudemer, Y. (2015). Generic along-strike segmentation of Afar normal faults, East Africa: Implications on fault growth and stress heterogeneity on seismogenic fault planes. *Geochemistry, Geophysics, Geosystems*, *16*(2), 443–467. doi: 10.1002/2014GC005691

Mann, C. J. (1993). Uncertainty in geology. In J. C. Davis & U. C. E. Herzfeld (Eds.), *Computers in geology—25 years of progress* (pp. 241–254). Oxford University Press, Inc.

Manzocchi, T., Heath, A., Childs, C., Telles, I., & Carneiro, M. (2019). Modelling fault zone displacement partitioning for risking across-fault juxtaposition. In *81st eage conference and exhibition 2019.*

Munthe, K., Holden, L., Mostad, P., & Townsend, C. (1994). Modelling sub-seismic fault patterns using a Marked Point Process. In *Ecmor iv-4th european conference on the mathematics of oil recovery.* doi: 10.3997/2214-4609.201411151

Nicol, A., Walsh, J., Childs, C., & Manzocchi, T. (2020). The growth of faults. In *Understanding faults* (pp. 221–255). Elsevier.

Nixon, C. W., Sanderson, D. J., & Bull, J. M. (2011). Deformation within a strike-slip fault network at Westward Ho!, Devon UK: Domino vs conjugate faulting. *Journal of Structural Geology*, *33*(5), 833–843. doi: 10.1016/j.jsg.2011.03.009

Osypov, K., Yang, Y., Fournier, A., Ivanova, N., Bachrach, R., Yarman, C. E., ... Woodward, M. (2013). Model-uncertainty quantification in seismic tomography: Method and applications. *Geophysical Prospecting*, *61*(6), 1114–1134.

Pakyuz-Charrier, E., Lindsay, M., Ogarko, V., Giraud, J., & Jessell, M. (2018, April). Monte Carlo simulation for uncertainty estimation on structural data in implicit 3-D geological modeling, a guide for disturbance distri-

bution selection and parameterization. *Solid Earth*, *9*(2), 385–402. doi: 10.5194/se-9-385-2018

Pakyuz-Charrier, E., Jessell, M., Giraud, J., Lindsay, M., & Ogarko, V. (2019). Topological analysis in monte carlo simulation for uncertainty estimation. *Solid Earth Discussions*, *2019*, 1–37. doi: 10.5194/se-2019-78

Peacock, D., & Sanderson, D. (1991). Displacements, segment linkage and relay ramps in normal fault zones. *Journal of Structural Geology*, *13*(6), 721–733. doi: 10.1016/0191-8141(91)90033-F

Ragon, T., Sladen, A., & Simons, M. (2018). Accounting for uncertain fault geometry in earthquake source inversions–i: theory and simplified application. *Geophysical Journal International*, *214*(2), 1174–1190.

Richards, F. L., Richardson, N. J., Bond, C. E., & Cowgill, M. (2015). Interpretational variability of structural traps: implications for exploration risk and volume uncertainty. *Geological Society, London, Special Publications*, *421*(1), 7–27. doi: 10.1144/SP421.13

Riesner, M., Durand-Riard, P., Hubbard, J., Plesch, A., & Shaw, J. H. (2017, May). Building Objective 3D Fault Representations in Active Tectonic Settings. *Seismological Research Letters*, *88*(3), 831-839. doi: 10.1785/0220160192

Rivenæs, J. C., Otterlei, C., Zachariassen, E., Dart, C., & Sjøholm, J. (2005). A 3D stochastic model integrating depth, fault and property uncertainty for planning robust wells, Njord Field, offshore Norway. *Petroleum Geoscience*, *11*(1), 57–65. doi: 10.1144/1354-079303-612

Røe, P., Georgsen, F., & Abrahamsen, P. (2014). An uncertainty model for fault shape and location. *Mathematical Geosciences*, *46*(8), 957–969.

Rosenbaum, M. S., & Culshaw, M. G. (2003). Communicating the risks arising from geohazards. *Journal of the Royal Statistical Society: Series A (Statistics in Society)*, *166*(2), 261–270. doi: 10.1111/1467-985X.00275

Rotevatn, A., Jackson, C. A.-L., Tvedt, A. B., Bell, R. E., & Blækkan, I. (2018, Au-

gust). How do normal faults grow? *Journal of Structural Geology*. doi: 10.1016/j.jsg.2018.08.005

Sanfeliu, A., & Fu, K.-S. (1983). A distance measure between attributed relational graphs for pattern recognition. *IEEE transactions on systems, man, and cybernetics*(3), 353–362.

Schaaf, A., & Bond, C. E. (2019). Quantification of uncertainty in 3-d seismic interpretation: implications for deterministic and stochastic geomodelling and machine learning. *Solid earth*.

Schaeffer, S. E. (2007). Graph clustering. *Computer science review*, *1*(1), 27–64. doi: 10.1016/j.cosrev.2007.05.001

Scheidt, C., Li, L., & Caers, J. (2018). *Quantifying uncertainty in subsurface systems* (Vol. 236). John Wiley & Sons.

Schneeberger, R., de La Varga, M., Egli, D., Berger, A., Kober, F., Wellmann, F., & Herwegh, M. (2017). Methods and uncertainty estimations of 3-d structural modelling in crystalline rocks: a case study. *Solid Earth*, *8*(5), 987. doi: 10.5194/se-8-987-2017

Seiler, A., Aanonsen, S. I., Evensen, G., & Rivenæs, J. C. (2010). Structural surface uncertainty modeling and updating using the ensemble Kalman filter. *SPE Journal*, *15*(04), 1–062. doi: 10.2118/125352-PA

Sepúlveda, I., Liu, P. L.-F., Grigoriu, M., & Pritchard, M. (2017, September). Tsunami hazard assessments with consideration of uncertain earthquake slip distribution and location: TSUNAMI HAZARD AND UNCERTAIN EARTHQUAKES. *Journal of Geophysical Research: Solid Earth*, *122*(9), 7252-7271. doi: 10.1002/2017JB014430

Smith, T. F., & Waterman, M. S. (1980). New stratigraphic correlation techniques. *The Journal of Geology*, *88*(4), 451–457.

Stoyan, D., & Gloaguen, R. (2011, August). Nucleation and growth of geological faults. *Nonlinear Processes in Geophysics*, *18*(4), 529–536. doi: 10.5194/npg-18

-529-2011

Suzuki, S., Caumon, G., & Caers, J. (2008). Dynamic data integration for structural modeling: model screening approach using a distance-based model parameterization. *Computational Geosciences*, *12*(1), 105–119. doi: 10.1007/s10596-007-9063-9

Tal, Y., Hager, B. H., & Ampuero, J. P. (2018, January). The Effects of Fault Roughness on the Earthquake Nucleation Process. *Journal of Geophysical Research: Solid Earth*, *123*(1), 437-456. doi: 10.1002/2017JB014746

Tarantola, A. (2006). Popper, Bayes and the inverse problem. *Nature physics*, *2*(8), 492–494. doi: 10.1038/nphys375

Thibaut, M., Gratier, J. P., Léger, M., & Morvan, J. M. (1996). An inverse method for determining three-dimensional fault geometry with thread criterion: Application to strike-slip and thrust faults (Western Alps and California). *Journal of Structural Geology*, *18*(9), 1127-1138.

Thiele, S. T., Jessell, M. W., Lindsay, M., Wellmann, J. F., & Pakyuz-Charrier, E. (2016, October). The topology of geology 2: Topological uncertainty. *Journal of Structural Geology*, *91*, 74-87. doi: 10.1016/j.jsg.2016.08.010

Thore, P., Shtuka, A., Lecour, M., Ait-Ettajer, T., & Cognot, R. (2002). Structural uncertainties: Determination, management, and applications. *Geophysics*, *67*(3), 840–852. doi: 10.1190/1.1484528

Torabi, A., & Berg, S. S. (2011). Scaling of fault attributes: A review. *Marine and Petroleum Geology*, *28*(8), 1444–1460. doi: 10.1016/j.marpetgeo.2011.04.003

Tvedt, A. B., Rotevatn, A., & Jackson, C. A. (2016). Supra-salt normal fault growth during the rise and fall of a diapir: Perspectives from 3D seismic reflection data, Norwegian North Sea. *Journal of Structural Geology*, *91*, 1–26. doi: 10.1016/j.jsg.2016.08.001

Wellmann, J. F., & Caumon, G. (2018, Nov). 3-D structural geological models: Concepts, methods, and uncertainties. In I. S. C. (Ed) (Ed.), *Advances in geo-*

physics (Vol. 59, p. 1-121). Elsevier. doi: 10.1016/bs.agph.2018.09.001

Wellmann, J. F., Horowitz, F. G., Schill, E., & Regenauer-Lieb, K. (2010, July). Towards incorporating uncertainty of structural data in 3D geological inversion. *Tectonophysics*, *490*(3-4), 141–151. doi: 10.1016/j.tecto.2010.04.022

Wellmann, J. F., Lindsay, M., Poh, J., & Jessell, M. (2014). Validating 3-D structural models with geological knowledge for improved uncertainty evaluations. *Energy Procedia*, *59*, 374–381. doi: 10.1016/j.egypro.2014.10.391

Wilson, C. G., Bond, C. E., & Shipley, T. F. (2019). How can geologic decision making under uncertainty be improved? *Solid earth*, 1–34.

Wood, D. R. (2007, June). On the Maximum Number of Cliques in a Graph. *Graphs and Combinatorics*, *23*(3), 337-352. doi: 10.1007/s00373-007-0738-8

Wu, X., Geng, Z., Shi, Y., Pham, N., Fomel, S., & Caumon, G. (2019, October). Building realistic structure models to train convolutional neural networks for seismic structural interpretation. *GEOPHYSICS*, 1-48. doi: 10.1190/geo2019-0375.1

Yielding, G. (2016). The geometry of branch lines. *Geological Society, London, Special Publications*, *439*, SP439–1. doi: 10.1144/SP439.1

Zakian, P., Khaji, N., & Soltani, M. (2017, October). A Monte Carlo adapted finite element method for dislocation simulation of faults with uncertain geometry. *Journal of Earth System Science*, *126*(7), 105. doi: 10.1007/s12040-017-0878-z

Zehner, B., Börner, J. H., Görz, I., & Spitzer, K. (2015, June). Workflows for generating tetrahedral meshes for finite element simulations on complex geological structures. *Computers & Geosciences*, *79*, 105-117. doi: 10.1016/j.cageo.2015.02.009

Zhu, S., Hack, R., Turner, K., & Hale, M. (2003). How far will uncertainty of the subsurface limit the sustainability planning of the subsurface? In *Proc. sustainable development & management of the subsurface (sdms) conference* (pp.

1033 5–7).